The ISCCP Atmospheric Temperature-Humidity Profile Data Product

William B. Rossow and Cindy B. Pearl
CREST Institute at the City College of New York

June 2018

Abstract

A new global atmospheric temperature-humidity profile data product is described that is based on a new retrievals from re-calibrated HIRS measurements with time interpolations to provide global coverage every 3 hr over the period 1980 – 2014. The new retrievals differ from previous analyses of satellite HIRS measurements in four ways: (1) a cloud detection algorithm is applied to each individual field of view (pixel) and all clear pixels are processed, (2) the retrieval procedure accounts for variations of CO_2 abundance over the record, (3) the retrieval procedure accounts explicitly for variations of surface topography and (4) the retrieval obtains values for near-surface air and skin temperatures separately. This paper reports the adaptation of these new retrieval results by employing time-interpolation procedures, including a specific statistical model of the diurnal variations of temperature in the lower troposphere over land, to estimate a globally complete set of profiles at 3-hr intervals. The humidity profile is extended into the stratosphere by combining the HIRS-based results with those from other satellite measurements of humidity. The resulting new product is compared with several other commonly used products.

1. Introduction

Measurements of atmospheric temperature-humidity profiles to monitor and forecast weather have been collected routinely by conventional means (radiosondes) since at least the late 1940s (*e.g.*, Eskridge *et al.* 1995, *cf.* Lanzante *et al*. 2003) and by satellites since the early 1970s (*e.g.*, Shi *et al.* 2008, Shi and Bates 2011). Yet for all the interest in these two variables from both a weather and climate change perspective, the most extensive products available have several well-known limitations, some of which could be mitigated. The products based solely on conventional measurements essentially cover only land areas, mostly in the northern hemisphere, and, not only do not resolve diurnal variations over land, but also are actually diurnally aliased because routine measurements are made twice daily (typically) at the same time UTC, representing different local times of day at different longitudes. This procedure introduces a systematic, longitudinally (and seasonally) varying bias in the data record (*cf.* Seidel *et al.* 2005 for magnitude estimates of diurnal variability), which is exacerbated by instrumental effects that introduce a daytime bias (*e.g.*, Sherwood *et al.* 2005). There are also systematic differences, especially for humidity measurements, between different radiosonde instruments operated in different countries (Gaffen 1994, Wang *et al.* 2003, Wang and Zhang 2008, Ho *et al.* 2010, Sun *et al.* 2010). In particular radiosonde humidity measurements at very cold temperatures (< 253 K) are generally biased low due to decreasing sensitivity (see discussion and references in Miloshevich *et al.* 2006 and McMillin *et al.* 2007 concerning comparison of radiosonde and satellite humidity determinations).

Earlier products based on satellite infrared measurements (see summary in Shi *et al.* 2016), which provide global coverage in principle, are limited to clear conditions (typically about 30% coverage when accumulated over a day) and are also diurnally aliased in a different way because these instruments are flown on satellites in sun-synchronous orbits providing a limited sample at the same local times of day at all longitudes. Because of clouds, these infrared-based products do not even provide complete global coverage at daily time intervals and are biased to clear conditions – in particular humidity is likely underestimated (Gaffen and Elliott 1993). Although profiling down to cloud top is possible, only completely clear or partially cloudy scenes are usually processed. The addition of microwave temperature sounding measurements in 1979 helped alleviate the cloud problem at the expense of lower vertical resolution; microwave humidity-sounding measurements were added in the late 1990s. However, a truly integrated joint analysis of the infrared and microwave measurements is not usually performed; instead the microwave measurements are usually used to "cloud-clear" the infrared measurements. The diurnal aliasing of these satellite-based measurements has been reduced somewhat by maintaining two polar orbiting satellites since the 1980s, providing four samples per day (in principle).

Three other problems with many of the available global products from satellite measurements are: (1) the retrieval methods usually do not account for variable topography (which could include variable cloud top pressure) – results for higher-topography locations are either not accurate or are not reported, (2) the diurnally and seasonally varying differences between surface skin temperature and near-surface air temperature are not accommodated in the retrieval which leads to diurnally and seasonally varying biases in the lowermost temperature and humidity profiles, and (3) the long-term records are not homogeneous because both the instruments and the analysis methods have changed over time without re-processing of the prior record (*cf.* Zhang *et al.* 2004, 2006 and references therein). Some efforts have begun to address this last issue, notably the NOAA Climate Data Record program in the US and the Satellite Application Facility – Climate Monitoring activities in Europe.

Many of these problems are supposed to be mitigated by the reanalyses, which at least remove the changes of the assimilation methodology over the time record but do not remove the changes of input data over the record. These results are also limited by the assimilation of diurnally aliased, land-based radiosondes and diurnally aliased "clear sky" satellite radiances -- that the diurnal aliasing of the radiosondes and satellites is different may also produce additional errors. Moreover, the use of clear-sky satellite radiances is evaluated against land-based radiosondes, which may produce biases over oceans. These assimilations also use SST products that are designed to represent "in-ocean bulk or mixed layer" temperatures that are neither skin nor near-surface air temperatures, whereas the radiosonde and satellite temperatures over land do not well represent the air temperatures right at the surface.

The temperature and humidity errors associated with the above issues are not quantitatively large (very roughly 1-3 K for temperatures and 10-25% for relative humidity, see discussion in Section 4), but attempts to use these products to determine surface longwave radiative, latent and sensible heat fluxes have demonstrated the large sensitivity of these estimates to small errors in the surface atmosphere properties, particularly temperature (Zhang *et al.* 2004, Vinukollu *et al.* 2011, Clayson and

Bogdanoff 2013). For example, a 1K error in near-surface temperatures produces a global mean error in downwelling longwave radiative flux at the surface of more than 8 W/m^2 and a 10% error in lower atmosphere specific humidity produces a global mean flux error of about 6 W/m^2 (Zhang *et al.* 1995). Moreover, these temperature-humidity errors (clear-sky and diurnal aliasing) are not random but systematic and dominate the errors in these flux products (*cf.* Zhang *et al.* 2006).

We report here on the development of a new temperature-humidity profile data product that is based on a new analysis of the multi-decadal infrared radiance measurements from the High-resolution Infrared Radiometer Sounder (HIRS) that have been re-calibrated to improve record homogeneity. Our new product provides a more homogeneous time record that is globally complete, treats the cloud contamination and near-surface atmosphere more carefully, and represents diurnal variability. This product, developed as part of a new set of the International Satellite Cloud Climatology Project (ISCCP) products, is called NNHIRS, and covers the globe on a 1.0-degree-equivalent-equal-area grid at 3-hr intervals from 1980 to present (the product is now being extended beyond 2014).

Section 2 describes the basic retrieved temperature-humidity profiles that are used, together with a stratospheric humidity product, to provide estimates of temperature-humidity profiles from 10 mb to the surface with complete global coverage at 3-hr intervals covering the time period 1980-2014. Also described are several other data products used to refine the basic products or to evaluate our final product. Section 3 describes how the two basic products are modified and combined to achieve the goal of globally complete coverage at 3-hr intervals. Section 4 evaluates the resulting product against other global products. Section 5 discusses some remaining limitations and indicates aspects that can be further improved.

2. Datasets

a. New analysis of HIRS measurements

The basic temperature-specific humidity (T-Q) profiles are obtained from a new analysis of the operational HIRS measurements on polar orbiting weather satellites (see Table 1 list of satellites). We refer to this product here as New HIRS (Shi *et al.* 2016) to distinguish it from our version called NNHIRS. The radiances that are used have been newly re-calibrated to reduce biases between instruments (Shi 2001, Shi *et al.* 2008, Shi and Bates 2011, Shi *et al.* 2016). Temperature profiles are determined from the surface to 50 mb and specific humidity profiles are determined from the surface to about 300 mb (Table 2). The T-Q profile retrieval is performed by a set neural networks, trained by a radiative transfer model, RTTOV Version 9 (Saunders *et al*. 1999, Matricardi and Saunders 1999, *cf.* Saunders *et al.* 2007), to use all wavelengths measured by HIRS; different networks are used for upper air temperature, upper air specific humidity and near-surface temperature and humidity. This version (Shi *et al.* 2016) is a further development of the method first reported in Shi (2001). Because of the long time period covered by this analysis, changes in CO_2 abundance systematically affect the results, so this analysis corrects for this effect.

The New HIRS analysis has several novel features compared with most previous methods. (1) A cloud algorithm is applied to each HIRS pixel (field-of-view), instead of

taking the warmest two profiles in a larger area or employing a comparison between HIRS and a microwave sounder radiances, thus all clear pixels (10-20 km in size at nadir) are processed to retrieve T-Q profiles. In a region with no clouds, results are obtained at spatial intervals as small as about 20 km. The cloud detection algorithm is patterned after the D-Version ISCCP IR algorithm and applied to HIRS channel 8 at a wavelength near 10 μm (Jackson *et al*. 2003). An additional check for cloud contamination is performed by comparison to coincident and collocated PATMOS-x cloud cover results from the AVHRR (Heidinger *et al.* 2014) on the same satellites as the HIRS instrument, if available (see Table 1). (2) The surface skin temperature (using realistic surface emissivities from ISCCP, Table 3) is retrieved as a separate quantity from the near-surface air temperature. (3) Near-surface air temperature and specific humidity, representing values at 2 m, are retrieved explicitly. (4) Variable topography is accounted for by training different neural networks for each surface pressure range. Surface pressure is estimated using the ISCCP TOPO dataset at 1.0-degree using the simplified barometric relation: PS = 1013.25 − 9.81 x 1.275 x Z/100 mb, where Z is topographic height in meters used as an estimate of geopotential height.

A post-retrieval adjustment of the profiles is performed by comparisons with collocated and coincident measurements of temperature and humidity by the RS92 collection of radiosondes in the troposphere and of temperature in the stratosphere by the GPS-RO (see Shi *et al.* 2016 for references).

HIRS data from all available satellites are analyzed (Table 1); hence, observations are obtained from two satellites (up to four samples per day in principle) for most of the time period. There are four short periods (1979-1980, 1985, 1997 and 2000) when only one satellite was available (two samples per day) and a 2-year period (2002-2004) when four satellites were available (eight samples per day). The 8-yr period, 02/2001 to 01/2009, which had three or four satellites operating, is used to develop the diurnal temperature variation model and a climatology that are used for filling missing observations (see Section 3h).

b. Stratospheric Water and Ozone Satellite Homogenized database (SWOOSH)

The HIRS-based specific humidity profiles are extended into the upper troposphere and stratosphere using specific humidity profiles obtained from a monthly mean climatology constructed from measurements by SAGE II and III from 1984 through 2005 and extended by UARS HALOE and the UARS and AURA MLS measurements to 2015. This product is called the Stratospheric Water and Ozone Satellite Homogenized data set (SWOOSH, Davis and Rosenlof 2016, http://www.esrl.noaa.gov/csd/groups/csd8/swoosh/189401-201312). The monthly mean values are mapped in a 5-degree latitude by 20-degree longitude map grid. Specific humidity values are reported at 31 pressure levels (Table 2).

c. Integrated Surface Database (ISD)

The HIRS-retrieved near-surface air temperatures (TA) and specific humidities (QA) over land were compared (after filters are applied, see Section 3e) with time-location-matched measurements from the global ISD collection of 3-hourly surface weather reports (Smith *et al.* 2011) for the period 2001 through 2009. Shi *et al.* (2016) also conducted such a comparison but limited it to the US Climate Reference Network subset of stations. The ISD surface relative humidity values (RHA) are converted to QA values using the reported values of TA and the formulae used to convert New HIRS Q values to RH (see Section 3i).

d. SEAFLUX

The HIRS-retrieved values of TA and QA over oceans were compared (after filters are applied, see Section 3e) with time-location-matched monthly-diurnal average determinations from the SeaFlux V1.1 product over oceans (Clayson *et al.* 2012, Clayson and Bogdanoff 2013) for the period 2002 through 2007. This product is a merged analysis of infrared and microwave determinations of SST, TA and QA that uses 3-hourly surface SW fluxes from GEWEX SRB (Gupta *et al.* 2006) to estimate the diurnally varying surface skin temperature from an SST product. Results are reported on a 1.0 degree equal-angle grid.

e. Analyzed RadioSounding Archive (ARSA)

Comparisons of NNHIRS T-Q profiles over land were made with time-location-matched radiosonde profiles (usually twice daily) from the ARSA collection for the period 2002 through 2008 (Analyzed Radiosoundings Archive (ARSA) v2., thanks to ARA/ABC(t)/LMD group for producing and making available the ARSA database, http://ara.abct.lmd.polytechnique.fr/index.php?page=arsa). For this comparison T and Q values at the 900 mb level are compared with NNHIRS because ARSA does not provide QA measurements (see Section 4a). The ARSA reported RH values are converted to Q values using the same formulae used for NNHIRS (see Section 3i).

f. Atmospheric Infrared Sounder (AIRS)

We compare the final NNHIRS product with the time-location-matched global AIRS T-Q profile Level 2 product (V6 L2 , Chahine *et al.* 2006, http://disc.sci.gsfc.nasa.gov/AIRS/documentation/v6_docs), which provide twice-daily sampling (in principle) for cloud-free or partially cloudy conditions (*cf.* Kahn *et al.* 2014). AIRS results are reported at 50x50 km intervals. Examples of the comparisons are shown for January and July 2007 (see Section 4a).

g. European Center for Medium-range Weather Forecasts Reanalysis -- Interim (ERA-I)

We compare the final NNHIRS product with the time-location-matched, global, daily T-Q profiles estimated in ERA-I (Simmons *et al.* 2007 and Dee *et al.* 2011) obtained from (http://www.ecmwf.int). ERA-I results are reported on a 1.5 degree equal-angle grid. Note that for the subset of ERA-I that we use, AIRS clear sky radiances were one of the assimilated datasets. Examples of the comparisons are shown for January and July 2007 (see Section 4a).

3. Modification and Merging Procedures

a. Characteristics of basic products

Since the basic New HIRS product is obtained from satellite infrared measurements, there are two inherent limitations: (1) detector technology (*e.g.*, Goody and Yung 1989) reduces the sensitivity to variations of Q at both very small values (< about 0.1 g/kg) and at very large values (> about 14 g/kg) and (2) clouds frequently interfere with measurements of some part of the profile. The limited sensitivity at small Q explains the termination of the Q profile at about the 300 mb level (*cf.* Fetzer *et al.* 2008) but also explains a few spuriously small values found in the polar regions, especially over Greenland and Antarctica, even at the surface. The limited sensitivity at large Q (saturation effect) explains the low bias of QA values found in the tropics by comparison to a microwave-based analysis (SEAFLUX, see Section 3c).

For a typical 2-satellite period (4 samples per day possible), there is on average 3 to 10% coverage (ocean and land, respectively) by the original observations at 3 hour time intervals because of cloud interference and only about 10 to 45% coverage for a daily accumulation (in this case, the average of at least one daytime and one nighttime original observation). Thus, the depiction of the space-time variations of the atmospheric temperature and humidity by such measurements does not completely resolve synoptic variations, both spatially and temporally, is clear-sky biased, and does not resolve the diurnal variations especially over land areas. Hence to achieve complete global coverage with diurnal resolution requires substantial time interpolation (see Section 3h).

Three other artifacts in the New HIRS product were discovered. Separate neural networks were applied in the northern and southern hemispheres, which led to an offset of Q values at the equator. A smoothing procedure was applied by averaging over ±10° of latitude (Shi *et al.* 2016), but this procedure did not entirely eliminate the offset, which is still about 1 g/kg at the surface. The second feature is a spurious diurnal cycle of Q in the lower atmosphere over land, particularly noticeable in desert areas (Figure 1), which we believe is caused by training the neural networks without considering a wide range of values for (TS −TA, skin minus air surface temperatures). The third feature is the occurrence of a few sudden, but localized, changes in Q values over oceans, which we believe are residual cloud contamination effects (see Sections 3e and 3h).

Because satellite sounders have difficulty resolving the near surface atmospheric properties, we compared the New HIRS results to two surface datasets to evaluate any systematic errors. Over land we used the time-location-matched 3-hourly ISD measurements of TA and QA and over oceans we used the time-location-matched monthly-diurnal mean TA and QA values from the SeaFlux product.

b. ISD comparison

The near-surface temperatures (TA) over land from the New HIRS (mapped to 1.0 degree-equivalent-equal area) compare reasonably well overall with ISD (point measurements within each matched map grid), with a spatial correlation of about 0.93 and rms differences about 4 K; but they are found to have a small temperature-dependent bias with respect to the ISD dataset (global mean difference, ISD minus New HIRS, about −1.5 K). This bias causes a systematic, seasonally varying, latitudinal difference pattern related to small overestimates for ISD values of TA > 300 K and TA < 230 K and small underestimates in between (Figure 2). These differences are especially noticeable at the cold extreme where New HIRS values are about 10 K higher than ISD values, which produces wintertime near-surface temperature inversions that are too weak. The near-surface specific humidities (QA) from New HIRS (daily minimum over land) show good agreement (spatial correlation about 0.85, bias about − 0.68 g/kg, rms difference about 2.5 g/kg) with ISD values with a small tendency to underestimate values at lower and higher temperatures.

c. SEAFLUX comparison

The TA values over ocean from New HIRS (mapped to 1.0 degree-equivalent-equal area) are in good agreement with the SEAFLUX values (spatial correlation about 0.99, bias about +0.3 K, rms difference about 1.6 K) with a tendency to be slightly larger in the subtropics, especially in the more cloudy regions (which could be a clear-sky bias). Even the extreme values for January and July 2007 agree within about 1 K. However the New HIRS QA values, though comparing favorably overall with SEAFLUX values (spatial correlation about 0.98, bias about +0.4 g/kg, rms difference about 1.3 g/kg), exhibit systematic geographic biases relative to the SEAFLUX values that amount to small overestimates for SeaFlux values of 8 g/kg < QA < 14 g/kg and larger underestimates for QA > 14 g/kg (Figure 3). These biases produce a systematic underestimate in the deep tropics, an overestimate in the subtropics and lower midlatitudes. This bias pattern does not exhibit significant seasonal dependence.

d. SWOOSH comparison

We use the SWOOSH product to extend the New HIRS Q profiles into the upper troposphere and stratosphere (see Section 3g for a description of the merger procedure). To check the consistency of these two products in the upper troposphere, the monthly mean SWOOSH Q values were compared with the New HIRS values at the overlapping pressure levels (with interpolation to common pressure levels). In addition distributions of the differences in specific humidity between different pairs of pressure levels were

examined to find those that showed (almost entirely) positive differences between the New HIRS values at a higher pressure (only New HIRS levels that actually report non-zero values are used in this comparison) and the SWOOSH values at a lower pressure. The New HIRS values at 260 mb or 320 mb (almost) always exceed those in the stratosphere at 100 mb. We also note that when the Q values from SWOOSH at pressures > 100 mb are converted to RH using the New HIRS temperatures, the values were found to be excessively large (sometimes >> 200%), even considering the large supersaturations with respect to ice that have been observed (*e.g.* Jensen *et al.* 2001), whereas the New HIRS values of Q near 300 mb, when converted to RH, are much better behaved (Figure 4 shows the ratio of SWOOSH to New HIRS RH values at 316 mb).

e. Filters

All available profiles of temperature (T) and specific humidity (Q) from New HIRS are collected in monthly histograms in the 1.0-degree ISCCP equal-area grid. Simple additional cloud-clearing procedures were applied to eliminate some remaining cloud contamination that was concentrated in (known) very cloudy locations, especially over oceans (based on the ISCCP cloud products, Rossow and Schiffer 1999). Most (but not all) of the removed profiles were also marked as probably cloud contaminated by the original New HIRS analysis cloud check flag. In addition a few unusually hot profiles were discovered over oceans so these were also removed. The tests to do these removals are applied to TA values; the whole T-Q profile is removed if any test fails. For each 1.0-degree-equivalent-equal-area grid cell in each month, the 1st and 99th percentile values in the histograms are determined, called TA1 and TA99. Based on the ensemble-shapes of all of these histograms, extreme values well-separated from the main distribution are removed if profiles are removed for which either TA < (TA1 − 3K) or TA > (TA99 + 3K) are discarded (much less than 1%). Over oceans the histogram of filtered TA values for each month is then examined to identify the mode value (TAmode) and the value on the larger (hot) side of TAmode with a frequency of occurrence that is half that of the mode value, called TA50. Additional profiles are removed if either TA > TAmode + 2 (TA50 − TAmode) or TA < TAmode − 2 (TA50 − TAmode). In some instances, there is no TA50 available on the hot side of the mode, in which case the value with a frequency of occurrence of 70% of the mode on the cold side (TA70) is used and the cold-side test is TA < TAmode − 3 (TAmode − TA70). Over land the histogram of filtered TA values for each month is also examined to identify TAmode and TA50. Profiles are removed if TA < TAmode − 3 (TA50 − TAmode). These tests of the TA histogram shapes are based on earlier experience in developing the ISCCP cloud detection

algorithm that showed that the "clear side" of the distribution tended to have a nearly universal shape (Rossow and Garder 1993a, b).

The filtered temperature profiles are averaged over each day and then over all samples of each of the 12 months in the year for the period 02/2001-01/2009 to provide a climatology to be used in the filling procedure (see Section 3h). Very limited filling in longitude (at most a few degrees of longitude) is used to ensure the global completeness of the climatology.

f. Adjustments

All filtered profiles are labeled as being over land or over water using the 0.25-degree ISCCP land-water mask (TOPO dataset) and mapped into 1.0-degree equal-area global grids at hourly time intervals (centered on the local hour) for each day, where the observation time UTC is converted to local standard time (LST) based on UTC and longitude to the nearest hour. All profiles falling within a grid cell within one hour are averaged. If both land and water are present in the grid cell, profiles over each surface type are averaged and then these two are combined, weighted by the fractional areal coverage of land. If the 1.0-degree-equivalent-equal-area grid cell is called land (land fraction > 65%), then at least one profile over land is required otherwise no data are reported. Likewise if the 1.0-degree grid cell is called water (land fraction < 35%), at least one profile over water is required. If the grid cell is called coast (intermediate land fraction) then at least one profile over land and one over water are required. The available values of the surface specific humidity, QA, are examined for each day to determine the minimum values over land (to suppress the spurious diurnal variations) and the average value over ocean. The Q-profile containing the minimum QA over land is replicated to all other hours for that day whereas the whole profile of Q is the daily average at each level over ocean.

Some profiles are missing values near the surface because of small differences between the original surface pressure used in the original New HIRS retrieval and the values reported in this product (see below) that account for some temperature dependence. These missing values are filled by vertical interpolation as part of the re-projection of the profiles from the original New HIRS standard pressure levels to the NNHIRS standard pressure levels (Table 2). Temperatures are first converted to ISCCP standard count values (used to represent infrared brightness temperatures), which are approximately linear in radiometer-measured energy, and linearly interpolated in pressure (P). Each monotonic portion of the profile is interpolated separately and then joined smoothly. Some spuriously large T values that occur near the tropopause are eliminated and interpolation performed to replace them. Q values are filled by interpolation of log Q with log P. The T profile is extrapolated to the 10mb level and the Q profile is extrapolated to the 260 mb level (if necessary).

The surface pressure for each profile is adjusted slightly to account for the average effects of varying atmospheric temperature using the barometric equation assuming a temperature lapse rate of −6.5 K/km:

$$PS(Z) = 1013.25\,[(TA - 6.5 \times Z) / TA]^{5.25} \quad (1)$$

where PS is in millibars, Z in kilometers above mean sea level and TA in Kelvins is the monthly mean near-surface air temperature at each location over land. The original New HIRS profiles are truncated or extended slightly. In mixed land-water grid cells, the surface pressure is the weighted average of the land and water values (where Z = 0 over water). Inland lakes, where topographic information is available in TOPO, are treated as land areas for this purpose. The near-surface temperature (TA) and specific humidity (QA) values are retained from the original profiles with no adjustment. The tropopause pressure is identified by searching upwards in the temperature profile to the first level where the temperature increases by ≥ 1K, but this location is checked to determine if it represents the absolute minimum temperature of the whole profile. If no minimum is found, then a test for a lapse rate < 0.3 K/km is used to define the tropopause location. If both tests fail to identify a tropopause level, the tropopause pressure is set to 100 mb.

The near-surface temperatures (over land) and specific humidities (over ocean) are next slightly adjusted from the original profile values based on systematic differences found in the comparison to the ISD dataset over land and the SEAFLUX dataset over ocean.

The original New HIRS values of TA over land exhibited a systematic bias relative to ISD measurements representing overestimates for TA > 300 K and TA < 230 K and underestimates in between (Figure 2). Using the baseline 8-yr climatology period, a three-part fit to the differences as a function of New HIRS TA was obtained. This fit was done for the 8-yr average of each month of the year to better represent the extremes (the annual average of the monthly fits is illustrated in Figure 2). Table 4 gives the fit functions used to adjust the New HIRS values of TA over land. This correction mainly reduced the overall bias to −0.5 K but did not significantly change the rms differences (now about 4.1 K) or the spatial correlation (now about 0.94).

Likewise the New HIRS values of QA exhibited systematic geographic biases relative to the SEAFLUX dataset representing overestimates for 8 g/kg < QA < 14 g/kg and underestimates for QA > 14 g/kg (Figure 3). This bias did not exhibit significant

seasonal dependence, so an additive adjustment is made with a single empirical curve fit based on the overlapping time period (2002-2007):

$$QA = QA + (-0.0000954413 * QA^5 + 0.0044154760 * QA^4 - 0.0693240329 * QA^3 + 0.4368326825 * QA^2 - 1.0513608055 * QA + 0.8696176721) \quad (2)$$

This correction reduced both the QA bias (now about + 0.05 g/kg) and the rms differences (now about 0.8 g/kg): Figure 5 shows the effects over 2007 as an example.

g. Merger with SWOOSH Q profile

The New HIRS values at 260 mb or 320 mb (almost) always exceed those in the stratosphere at 100 mb. Since the SWOOSH documentation recommends using humidity values for pressures ≤ 100 mb, the two water vapor profiles were joined by interpolating log Q versus log P between the 100 mb level and the last level with non-zero values in the New HIRS product, generally the 320 mb level (see a typical example in Figure 6, such figures were examined for all seasons and latitude zones). The monthly SWOOSH profiles are replicated to each hour local time and for each 1.0-degree-equivalent-equal-area grid cell and then merged by vertical interpolation with the New HIRS profiles. In this fashion, the synoptic variations in the troposphere are weakly reflected into the lower stratosphere below the 100 mb level by the interpolation procedure.

h. Filling Missing Values

When four satellites are operating, the original observations cover about 6 to 34% (19% average) of the earth for each 3-hr interval during the day. The more usual situation is that observations are available from two satellites. To achieve the goal of adequate diurnal resolution and to compensate for the inhomogeneous time-of-day sampling over the whole time record, the temperature values from the 8-yr period (02/2001-01/2009) with three-to-four satellite coverage (six-to-eight samples per day) were fit by an analysis of the diurnal variations for each month of the year at each geographic location at each pressure level (*cf.* Lindfors *et al.* 2011). The analysis has two steps. First, the monthly mean diurnal anomalies (deviations from the daily average over all times of day for each satellite separately) at local hour intervals are combined for all satellites and fit with a cubic spline (unless the temperature range is < 2 K or > 5 K over ocean and > 40 K over land, in which case a Piecewise Cubic Hermite Interpolation, PCHIP, method is used). The excessively large diurnal amplitudes over ocean and land are located in particular regions that are known to have extensive, persistent cloudiness. As part of the evaluation of the empirical fits, the standard deviation of the monthly-hour average anomaly values

for each grid cell and each month of the year are used to discard the one value farthest from the daily mean if it is more than two standard deviations from the mean and if its removal reduces the standard deviation by more than 20%. Second, a Principle Component Analysis is performed on the hourly anomalies from the daily mean temperature for each grid cell at each pressure level over the whole period 02/2001-01/2009 (*cf.* Aires *et al.* 2004). The final diurnal variation model uses only the first three PCs to smooth out the variations, which explains about 55% of the variance over oceans (where this procedure is not used) and about 94% over land (*cf.* Aires et al 2004). The rms differences between the 3-term and the all-term PCA representations were found to increase systematically as the diurnal amplitude decreased so the PCA model was restricted to locations where the diurnal range is ≥ 2 K: all land areas at pressure levels ≥ 500 mb. Generally diurnal variations over ocean and in the upper atmosphere were smaller than this cutoff. The PCA-based diurnal model is also used to determine bias corrections for determining the daily mean temperatures from a limited diurnal sample where time of day varies for different satellites over their lifetime.

Daily mean T profiles are determined for all days that have, at least, one daytime and one nighttime sample; the PCA-based bias corrections are applied to correct for the specific time-of-day of the available samples. The Q profiles are retained only for days with an existing daily mean T profile. Monthly averages of these T and Q profiles are also calculated.

For a 2-satellite period there is on average 10% original data over land for a 3 hour time period, so the T profile filling procedure starts with the daily mean value for each location (an average of about 45% of the cases). If a daily mean value is not available on a particular day, the daily mean is obtained by linearly interpolating from nearby daily mean values in a ±5-day interval (about 27% of the cases). If the interpolation fails because data are not available, the monthly averaged daily mean value is used (about 25% of the cases); if there is no monthly mean, then the climatology for the appropriate month is used (< 3% of the cases). The PCA-based diurnal model is then applied to the daily mean T profiles from the surface up to the 500 mb level. Values aloft are filled through linear interpolation in time (24 hours +/-5 days), if data are not available then daily mean or the climatology is used. Over ocean there is about 3% original data, about 66% is filled through linear interpolation between the closest available times regardless of time of day (over an interval +/- 5 days), about 22% is filled by the monthly mean, and about 11% by the climatological mean.

Humidity values for all hours on days with a daily mean T profile are already filled with the daily minimum value over land and the daily average over ocean. If the daily mean T profile is missing, the Q profile is replaced over land (ocean) by linear interpolation of daily minimum (mean) values over a ±5-day interval; if this interpolation fails, the monthly mean daily minimum Q profile is used. If the monthly mean Q profile is missing, the climatology from 02/2001-01/2009 of daily minimum (mean) Q values for the appropriate month is used.

The available stratospheric specific humidities are much sparser in the earliest years of the SWOOSH record; these are filled using a climatology based on the SWOOSH record from 2005-2014. The resulting monthly mean maps in 1° by 1° equivalent equal-area grid are replicated to each local hour of each day.

The now globally complete profiles of T and Q at 1-hr intervals in local time are finally reduced to a 3-hr UTC version by taking the hourly value closest to the center of the 3-hr time window based at the longitude of each grid cell. This approach produces a better-behaved diurnal temperature cycle over land but can mean that some original observations are dropped. However, the values reported are based on all the original observations through the daily mean value.

i. Change of Moisture Variable

To preserve precision over the whole range of specific humidity values, Q, they are converted to relative humidity, RH = Q/QS at each location and local hour using the hourly temperature values in formulae for e_s from Murphy and Koop (2005):

$$e_{s,l} = e_0 \exp\left[(\alpha - 1)\, e_6 + d_2 (T_0 - T) / TT_0 + d_3 \ln (T/T_0) + d_4 (T - T_0)\right], \qquad (3)$$

where $e_{s,l}$ is the saturation vapor pressure over liquid water for $T \geq T_0$, $T_0 = 273.15$ K, $e_0 = \exp(e_1 + e_6) = 6.091888$ mb, $\alpha = \tanh[e_5 (T - 218.8\ \mathrm{K})]$, $d_i = (e_i + \alpha\, e_{i+5})$ and the values of e_i are:

$e_1 = 6.564725$
$e_2 = -6763.22$ K
$e_3 = -4.210$
$e_4 = 0.000367$ K^{-1}
$e_5 = 0.0415$ K^{-1}
$e_6 = -0.1525967$
$e_7 = -1331.22$ K
$e_8 = -9.44523$
$e_9 = 0.014025$ K^{-1}

and

$$e_{s,i} = B \exp\left[b_1 (T_0 - T) / T_0 T + b_2 \ln (T/T_0) + b_3 (T - T_0)\right] \qquad (4)$$

where $e_{s,i}$ is the saturation vapor pressure over ice for $T < T_0$, $b_0 = 9.550426$, $b_1 = -5723.265$ K, $b_2 = 3.53068$, $b_3 = -0.00728332$ K^{-1} and

$$B = (10^5) \exp [b_0 + b_1/T_0 + b_2 \ln (T_0) + b_3 T_0] = 6.111536 \text{ mb} \quad (5)$$

The vapor pressures are converted to saturation specific humidity using

$$QS = 0.622\ e_s\ /\ (P - 0.378\ e_s) \quad (6)$$

Thus RH is determined with respect to liquid phase at and above freezing temperature (273.15 K) and with respect to ice phase below freezing. If the NNHIRS value of RH < 0.5% at any temperature, it is reset to 0.5%. If RH > 110% at T ≥ 273.15 K, then it is reset to 110%. If RH > 150% at T < 273.15 K, it is reset to 150%. The larger upper limit at lower temperatures is consistent with upper air humidity measurements indicating very large vapor supersaturations are required to initiate ice condensation (Jensen *et al.* 2001).

4. Evaluations of Final NNHIRS Product

a. Comparison to other products

Since the data products that we compare to the final NNHIRS product each have different space-time sampling intervals, the difference statistics reported below represent different space-time match-ups. For the ARSA comparison, the ARSA profiles (point measurements) are matched with the NNHIRS grid in which they are located and time matched to the nearest NNHIRS 3-hr interval. Hence the time difference between these two datasets can be as much as 1.5 hr and the spatial match-up is a point to an area. Sun *et al.* (2010) quantify differences between COSMIC GPS and radiosondes related to space-time mismatches: the standard deviation of the temperature differences increases by 0.35 K per 3 hr and 0.42 K per 100 km mismatch and of the relative humidity differences increase by 3.3% per 3 hr and 3.1% per 100 km mismatch. Thus we can expect rms differences of temperature and humidity that are as much as about 0.5 K and 4% larger just because of the space-time mismatch effect. For the AIRS comparison, the AIRS profiles at 50x50 km (Level 2) are averaged to the NNHIRS 1.0 degree equal-area grid and the AIRS overflight time matched to the nearest NNHIRS 3-hr interval. Hence, while the spatial match-up is accurate, the time difference between these two datasets can be as much as 1.5 hr. For the ERA-I comparison, the nearest NNHIRS grid cell and 3-hr time are matched to the ERA-I profiles. Hence, the space and time match-ups for these two are pretty accurate. All differences are reported as (OTHER minus NNHIRS).

The comparison results are illustrated by typical results for January and July 2007. Table 5 provides a global summary of the average and rms differences between NNHIRS and AIRS, ARSA (over land) and ERA-I, separated by land and water, at the surface (or 900 mb for ARSA) and at two other pressure levels (500 and 320 mb). Figures 7 and 8 show the average T-profile differences (Kelvins) of AIRS, ARSA and ERA-I with NNHIRS for July 2007 for water and land, respectively; Figures 9 and 10 show the average Q-profile differences (g/kg) of AIRS, ARSA and ERA-I with NNHIRS

for July 2007 for water and land, respectively (January 2007 is not shown because the differences are generally similar, but significant seasonal differences are discussed).

Turning first to temperatures over ocean, the average differences of both AIRS and ERA-I with NNHIRS are about +0.5 to +1.5 K, except below the 800 mb level and near the surface where they are about -0.5 to -1.5 K. The rms differences are 1.5 to 2.5 K, larger at mid-levels, and the average correlations are 0.97-0.99. Both AIRS and ERA-I TA values are cooler than the SeaFlux values in low and midlatitudes where the NNHIRS values are in better agreement. This difference could be due to the difference between conventional SST values and the diurnally-corrected surface skin temperatures in the SeaFlux product (Clayson and Bogdanoff 2013). In the polar regions, the AIRS temperatures are in better agreement with NNHIRS (within 1-2 K, colder in winter than summer) than the ERA-I values which are generally much warmer, especially at lower levels where the average difference is +3 to +5 K. Given the already weak temperature inversions in the NNHIRS product, this suggests that ERA-I either lacks such inversions in the winter polar regions or they are much less frequent. Both AIRS and ERA-I are colder than NNHIRS by 1-3 K near the tropopause and in the stratosphere in the tropics and in the winter polar regions.

Temperature differences over land, where the NNHIRS values of TA were adjusted to ISD, are a little larger than AIRS and ERA-I values: the average differences are about -0.75 to -2 K, differences are positive at mid-levels and negative at upper levels and near the surface. The rms differences are 1.5 to 3.5 K, larger near the surface, and the average correlations are a little lower, 0.90-0.99. Similar to the ocean profiles, the AIRS and ERA-I temperatures are warmer than NNHIRS aloft but cooler below the 800 mb level; ARSA shows similar differences with NNHIRS. Agreement among all the datasets is slightly better in July than January. Over the summer poles, AIRS and ERA-I are 3 K warmer/cooler (south/north) than NNHIRS at the surface decreasing to about zero difference at 100 mb (ARSA is probably unrepresentative over Antarctica); over the winter poles AIRS, ERA-I and ARSA 4-5 K warmer than NNHIRS near surface but 1-2 K cooler above the 400 mb level. Compared to ISD values of TA, NNHIRS is within 1-2 K except for southern midlatitudes, where NNHIRS is warmer by up to 3 K (also in January) and colder by about 3K in both polar regions in winter (January not shown).

The specific humidity comparison over oceans, where the NNHIRS values of QA have been adjusted to SeaFlux, shows average differences with AIRS and ERA-I of about -10% (roughly -1.0 g/kg) at the surface and about +30% aloft. The rms differences are about the same magnitude; correlations range from 0.93 to 0.99. Relative to NNHIRS at all latitudes in both seasons, AIRS & ERA-I grow progressively wetter than NNHIRS at lower levels, especially at 900 mb, but are drier at the surface, especially in the tropics. In this case, the SeaFlux values of QA agree better with the NNHIRS values (because of the adjustment) than with the AIRS and ERA-I values.

Over land the pattern of differences is similar to over oceans, where the average differences are +20% (roughly +1.5 g/kg) at surface and +30-40% aloft; the rms differences are similar in magnitude and the correlations range from 0.80 to 0.95. Again the AIRS and ERA-I, as well as those from ARSA, grow progressively wetter than NNHIRS at lower levels, especially at 800 mb. At the surface AIRS and ERA-I values of QA are in better agreement with ISD values; the NNHIRS values, which are the daily minimum from New HIRS, are drier than ISD. The somewhat drier profiles of NNHIRS

relative to both AIRS and ERA-I persist into the upper atmosphere and the polar regions and these differences are all similar in magnitude to those with respect to ARSA, despite the well-known dry bias of radiosondes at such cold temperatures.

b. Final uncertainty estimates

Shi *et al.* (2016) estimate temperature-humidity global mean uncertainties for their New HIRS retrievals of ±0.3 K and ±0.2 g/kg (depending on the pressure level), respectively, except at the lowest levels where they are as large as −1.0 K and −0.6 g/kg at 1000 mb level, respectively. The global rmse values are estimated to be about 2 K and 2 g/kg above the 750 mb level and about 4 K and 2.5 g/kg near the surface; near-surface rmse values are larger for temperatures (up to 4 K) in the polar regions and for specific humidities (up to 2.8 g/kg) in the tropics. These estimates refer to the uncertainties in the retrievals and do not account for space-time sampling effects, including the clear sky bias and diurnal bias, on the final representation of the atmospheric temperature-humidity profiles. We find structural differences with ISD and SeaFlux at the surface and with ARSA, AIRS and ERA-I aloft that are only a little larger.

Uncertainty estimates for the ISD measurements are difficult to find: the almost exclusive focus of recent research has been on long-term changes of record-anomalies rather than absolute values. Most authors presenting new results report their differences against the surface station data without discussing the measurement uncertainties in the latter. A guess is that the random temperature measurement uncertainties might be at least about ±1.0 K and the random humidity measurement uncertainties might be at least about ± 10% (larger at lower temperatures). In any case, a larger source of differences between the ISD values of TA and QA and values from a satellite product like NNHIRS are related to the space-time scale mismatches in the comparison: in our case, we compare a value representing a 100 x 100 km domains sampled near the center of a 3-hr time interval to measurements taken at the synoptic times but at one point somewhere in each domain. This suggests, based on Sun *et al.* (2010), that differences of at least 1.5 K and 20% could occur even for a perfect satellite product.

The SeaFlux uncertainties in TA and QA have been evaluated by comparison with a large collection of ship and buoy measurements (*cf.* Liu *et al.* 2011, Clayson *et al.* 2012): estimated rms uncertainties are 1.3 K for TA and 1.3 g/kg for QA.

Thus, we conclude that the differences between the NNHIRS values of TA and QA and the values from ISD and SeaFlux are consistent with the independently estimated uncertainties of both the New HIRS retrievals and these other measurements.

As summarized in Table 5, the average differences between NNHIRS and ARSA, AIRS and ERA-I are all about 1-2.5 K for T and 10-40% for Q, depending on pressure level. The radiosonde data (in this case the ARSA collection) are commonly taken as the

comparison standard for satellite products and reanalyses. However, there are many studies that show differences in accuracy among the different types of radiosondes included in such collections (*e.g.*, Gaffen 1994, Wang *et al.* 2003, He *et al.* 2009, Ho *et al.* 2010). For instance, Misloshevich *et al.* (2006) and McMillin *et al.* (2007) both illustrate such differences in comparison with matched AIRS retrievals. Also systematic differences of humidity measurements with temperature, particularly at the very cold temperatures in the upper troposphere and polar regions (*e.g.*, Wang and Zhang 2008) and day-night differences of temperature measurements (*e.g.*, Sherwood *et al.* 2005) have been noted. Taken all together, these and other studies suggest that the estimated uncertainties, in an rms sense, of a collection of radiosondes are at least about ± 1 K for T and ± 5-10% for Q in the lower troposphere and ± 10-20% in the upper troposphere.

Evaluations of AIRS T-Q profiles provide estimates of uncertainties (at the retrieval level) that are shown to be dependent on the cloud conditions (Chahine *et al.* 2006, Susskind et al 2006) and surface altitude (Ferguson and Wood 2010). The detailed assessment by Divakarla *et al.* (2006) reports for completely clear retrievals (see also Chahine *et al.* 2006) that the rms T differences with radiosondes are about 1.5 K, slightly smaller (< 1 K) over ocean and slightly larger (< 1 K) over land, slightly larger near the surface and above the 300 mb level and slightly smaller in between. For Q the rms relative differences increase monotonically from about 18% near the surface to about 40% at 300 mb, slightly smaller (< 5%) over oceans and slightly larger (< 5%) over land. The effect of partial cloudiness degrades the performance somewhat, increasing the rms differences by about 50% (relative). These rms differences are slightly smaller for the tropics and slightly larger in (north) polar regions. Biases of T are generally less than 1 K (negative near the surface, near 300 mb and above 100 mb level and positive near 650 mb and 200 mb) and biases of Q are about +5% between 500-700 mb and -15% above 400 mb. McMillin *et al.* (2007) show that these differences are smaller for nighttime comparisons than daytime comparisons, even when the radiosondes are adjusted using GPS-RO measurements, which suggests some diurnal difference in the AIRS retrievals.

ERA-I estimated uncertainties compared to radiosondes (which are assimilated) are similar in magnitude to the AIRS differences but less well-known away from the locations and times of the assimilated data. The profiles at these other locations and times depend on the assimilated satellite infrared radiances (ERA-I assimilates AIRS radiances from 2003 onwards), which are biased towards clear conditions but have additional uncertainties associated with the fidelity of the model radiation code and the general assimilation process to estimate temperatures and humidities for cloudy locations. The clear sky biases are season and location dependent: Q would be biased low (*cf.* Gaffen and Elliott 1993) and the T bias would be high in summer and low in winter, especially over land. These biases are also associated with the diurnally aliased nature of the assimilated measurements discussed in the Introduction. Dee *et al.* (2011) show rms departures of lower troposphere T and Q from the assimilated observations of about 0.7 K and 1.4 g/kg. Simmons *et al.* (2010) claim that the ERA-I values of QA over land are generally drier than surface measurements but moister than radiosonde measurements at lower levels – the stated magnitude of the latter difference is 0.2 g/kg. Noh *et al.* (2016) compared ERA-I to the GRUAN subset of radiosondes (remembering that these data are assimilated) and estimated mean (rms) uncertainties for T to be 0.2 (0.5-1.0) K and for RH to be 2-6% (10%), where they note a high bias of ERA-I RH values above the 500

mb level. Noh *et al.* (2016) also emphasize that the biases in ERA-I Q values are proportional to Q.

Overall the average differences of T in the NNHIRS product with all of these products appear to be within the uncertainties of other products and only a little larger than the New HIRS retrieval uncertainties. That both AIRS and ERA-I (and ARSA over land) have the same pattern of disagreement with NNHIRS T values may indicate that the NNHIRS product is slightly too cold aloft and too warm near the surface. The Q story is more complicated. The spatial pattern of the differences between New HIRS and SeaFlux QA values over oceans also appears in a comparison of AIRS and SeaFlux, though with somewhat smaller magnitude. Over land, the suppression of a spurious diurnal cycle of QA in the New HIRS retrievals by selecting the daily minimum value appears to have produced a low bias there. However, an evaluation of AIRS suggests that it is also biased low (clear sky bias), so the NNHIRS low bias may be worse than indicated in Figure 10. Note that ERA-I, which is also thought to be biased low over land, also appears to agree with the AIRS average difference. We note generally that AIRS appears to be wetter than ERA-I, which is in turn similar to ARSA over land, and that the NNHIRS values of Q are generally lower overall.

Most of these products are more uncertain in the upper troposphere and stratosphere, especially for Q. The estimated uncertainty in the SWOOSH humidities is ± 20% (Davis and Rosenlof 2016), whereas the estimated uncertainty for AIRS values at 300 mb level range from < 10% on average (≤ 30% rms) in the tropics to > 10% on average (40-70% rms) at higher latitudes and at lower pressures as compared with MLS measurements (Fetzer *et al.* 2008), but some of these differences are known to associated with MLS biases (see Fetzer *et al.* 2008 for more detail). The New HIRS stratospheric temperatures have been adjusted using GPS retrievals and are thought to be accurate to within ±1.0 K (Shi et al. 2016).

5. Discussion and Conclusions

Overall, we conclude that the NNHIRS T values are accurate to within 1-2 K aloft with TA being less accurate, especially over land, at 2-3 K. These uncertainties may be systematic in that the T profiles are a little cold aloft and a little warm near the surface. The NNHIRS Q values are accurate to within 20% aloft with QA being less accurate, especially over land, at 30%; in this case there is likely a dry bias near the surface over land. These uncertainty levels are sufficiently small that this product can be used for the study of the weather processes involved in weather and seasonal variability (keeping in mind the clear-sky bias, *cf.* how this is handled in Zhang *et al.* 2004).

We also show in Figure 11 the long-term, deseasonalized anomalies of the global monthly averages of TA and QA over land and ocean separately. The long-term record of TA anomalies exhibits no particular trend, but some notable changes, over land but does show a small systematic decrease by about 1 K over 35 years at the surface over oceans. On the other hand, anomalies of T values aloft, even at 900 mb, show no trend (not shown). The QA anomalies show downward trend over land and ocean of about 3-6%

(relative) over 35 years. No trend in Q values aloft is found in the mid-troposphere but a similar downward trend of about 4% (relative) over 35 years is found near the tropopause (not shown). Examination of the statistics from original new HIRS retrievals (Shi *et al.* 2016) shows similar features that appear to coincide with changes of instrument. Although some of this might be related to instrument calibration differences (see Shi *et al.* 2016 for more discussion and references), some of the difference is related to the progressive drift of the satellite orbits away from local maximum daytime temperature. That this effect plays a role is argued by the fact that the anomaly features are largest near the surface and that these differences are smaller over land in our version of the product that has been corrected (approximately) for differences of diurnal phase. We interpret these long-term variations, about 1 K for T and 5% for Q, as artifacts from the multi-instrument construction of the record; these variations are still within the estimated accuracies of our new product.

Among all of these products we note larger disagreements in several instances: (1) near-tropopause humidity and its weather-time-scale variability are not well determined, although GPS-RO-based products are beginning to improve the T values, (2) near-surface humidity over land is not well-determined from either conventional sources (incomplete spatial coverage) or satellite products (poor diurnal resolution, clear sky bias), (3) ocean near-surface humidity from satellite infrared measurements is poor at the largest tropical and lowest polar values and seems to overestimate QA in the subtropics.

Judged from the perspective of how accurately surface radiative and turbulent heat and water fluxes can be determined using any of these T-Q data products, we can say that their quality limits the accuracy of such flux determinations to something like 10-20 W/m^2 (*cf.* Zhang *et al.* 1995). This accuracy is sufficient for studying the weather-scale variations of these fluxes. Many of these products do not provide complete global coverage or sufficiently fine time resolution to characterize the diurnal, synoptic or even seasonal variations of these fluxes. In particular, that incomplete (and/or variable) space-time coverage can produce systematic errors has not been well-characterized in the uncertainty estimates. To improve our diagnosis of the atmosphere's energy and water exchanges for climate change studies requires reducing the rms T and Q uncertainties at 100 km, 3 hr scales to at least 1 K and 10% (relative), respectively. Our NNHIRS product, while providing complete global coverage at 3-hr intervals – resolving the diurnal variations better – does not meet these accuracy requirements nor does any other available product.

Acknowledgements: This work was supported by funding from the NASA MEASURES and NOAA Climate Data Record programs, by NASA grant NNX13AI22A and NSF Grant 1240643 (PD-06-5740). We thank Lei Shi and John Bates for discussions about their product and how to design this version. We thank testers of earlier and final versions: Y-C. Zhang, P.W. Stackhouse, C.A. Clayson and E.F. Wood.

References

Aires, F., C. Prigent and W.B. Rossow, 2004: Temporal interpolation of global surface skin temperature diurnal cycle over land under clear and cloudy conditions. *J. Geophys. Res.*, **109**, doi 10.1029/2003JD003527 (1-18).

Chahine, M.T., T.S. Pagano, H.H. Aumann, R. Atlas, C. Barnet, J. Blaisdell, L. Chen, M. Divakarla, E.J. Fetzer, M. Goldberg, C. Gautier, S. Granger, S. Hannon, F.W. Irion, M. Kakar, E. Kalnay, B.H. Lambrigsten, S-Y. Lee, J. Le Marshall, W.W. McMillan, L. McMillin, E.T. Olsen, H. Revercomb, P. Rosenkranz, W.L. Smith, D. Staelin, L. Larrabee Strow, J. Susskind, S. Tobin, W. Wolf and L. Zhou, 2006: AIRS: Improving weather forecasting and providing new data on greenhouse gases. *Bull. Amer. Meteor. Soc.*, **87**, 911-926, doi:10.1175/bams-87-7-911.

Clayson, C.A., J.B. Roberts and A.S. Bogdanoff, 2012: The SeaFlux Turbulent Flux dataset version 1.0 documentation. SeaFlux Project, 5pp. [available online at http://seaflux.org/seaflux_data/DOCUMENTATION/SeaFluxV1.0documentation.pdf].

Clayson, C.A., and A.S. Bogdanoff, 2013: The effect of diurnal sea surface temperature warming on climatological air-sea fluxes. *J. Climate*, **26**, 2546-2556, doi:10.1175/JCLI-D-12-00062.1.

Davis, S., and K. Rosenlof, 2016: NOAA ESRL Stratospheric Water and OzOne Satellite Homogenized (SWOOSH), Version 2. NOAA National Centers for Environmental Information (NCEI). doi:10.7289/V5TD9VBX.

Dee, D.P., and co-authors, 2011: The ERA-Interim reanalysis: Configuration and performance of the data assimilation system. *Quart. J. Roy. Meteor. Soc.*, **137**, 553-597.

Divakarla, M.G., C.D. Barnet, M.D. Goldberg, L.M. McMillin, E. Maddy, W. Wolf, L. Zhou and X. Liu, 2006: Validation of Atmospheric Infrared Sounder temperature and water vapor retrievals with matched radiosonde measurements and forecasts. *J. Geophys. Res.*, **111**, D09S15, doi:10.1029/2005JD006116, (1-20).

Eskridge, R., A. Alduchov, I. Chernykh, Z. Panmao, A. Polansky and S. Doty, 1995: A comprehensive aerological research data set (CARDS): Rough and systematic errors. *Bull. Amer. Meteor. Soc.*, **76**, 1759-1775.

Ferguson, C.R., and E.F. Wood, 2010: An evaluation of satellite remote sensing data products for land surface hydrology: Atmospheric Infrared Sounder. *J. Hydrometeor.*, **11**, 1234-1262, doi:10.1175/2010JHM1217.1.

Fetzer, E.J., W.G. Read, D. Waliser, B.H. Kahn, B. Tian, H. Vomel, F.W. Irion, H. Su, A. Eldering, M.T. Juarez, J. Jiang and V. Dang, 2008: *J. Geophys. Res.*, **113**, D22110, (1-17), doi:10.1029/2008JD010000.

Gaffen, D.J., 1994: Temporal inhomogeneities in radiosonde temperature records. *J. Geophys. Res.*, **99**, 3667-3676.

Gaffen, D.J., and W.P. Elliott, 1993: Column water vapor content in clear and cloudy skies. *J. Climate*, **6**, 2278-2287.

Goody, R.M., and Y.I. Yung, 1989: *Atmospheric Radiation: Theoretical Basis*, Oxford, 519pp.

Gupta, S.K., P.W. Stackhouse, S.J. Cox, J.C. Mikovitz and T. Zhang, 2006: Surface radiation budget project completes 22-year data set. *GEWEX News*, **6 (4)**, International GEWEX Project Office, 12-13.

He, W.Y., S.P. Ho, H.B. Chen, X.J. Zhou, D. Hunt and Y.H. Kuo, 2009: Assessment of radiosonde temperature measurements in the upper troposphere and lower stratosphere using COSMIC radio occultation data. *Geophys. Res. Lett.*, **36**, 1-7, doi:10.1029/2009GL038712.

Heidinger, A.K., M.J. Foster, A. Walther and X.P. Zhao, 2014: The Pathfinder Atmospheres-extended AVHRR climate dataset. *Bull. Amer. Meteor. Soc.*, **95**, 909-922.

Ho, S-P., X. Zhou, Y-H. Kuo, D. Hunt and J. Wang, 2010: Global evaluation of radiosonde water vapor systematic biases using GPS radio occultation from COSMIC and ECMWF analysis. *Remote Sens.*, **2**, 1320-1330, doi:10.3390/rs2051320.

Jackson, D.L., D.P. Wylie and J.J. Bates, 2003: The HIRS pathfinder radiance dataset (1979-2001). Presented at 12th Conference on Satellite Meteorology and Oceanography, *Amer. Meteor. Soc.*, Long Beach, CA, 10-13 Feb.

Jensen, E.J., O.B. Toon, S.A. Vay, J. Ovarlez, R. May, T.P. Bui, C.H. Twohy, B.W. Gandrud, R.F. Pueschel and U. Schumann, 2001: Prevalence of ice-supersaturated regions in the upper troposphere: Implications for optically thin ice cloud formation. *J. Geophys. Res.*, **106**, D15, 17,253-17,266.

Kahn, B.D., F.W. Irion, V.T. Dang, E.M. Manning, S.L. Nasiri, C.M. Naud, J.M. Blaisdell, M.M. Schreier, Q. Yue, K.W. Bowman, E.J. Fetzer, G.C. Hulley, K.N. Liou, D. Lubin, S.C. Ou, J. Susskind, Y. Takano, B. Tian and J.R. Worden, 2014: The Atmospheric Infrared Sounder version 6 cloud products. *Atmos. Chem. Phys.*, **14**, 399-426, doi:10.5194/acp-14-399-2014.

Lanzante, J.R., S.A. Klein and D.J. Seidel, 2003: Temporal homogenization of monthly radiosonde temperature data. Part I: Methodology. *J. Climate*, **16**, 224-240.

Lindfors, A.V., I.A. Meckenzie, S.F.B. Tett and L. Shi, 2011: Climatological diurnal cycles in clear-sky brightness temperatures from the High-resolution Infrared Radiation Sounder (HIRS). *J. Atmos. Ocean Technol.*, **28**, 1199-1205.

Liu, J., J.A. Curry, C.A. Clayson and M.A. Bourassa, 2011: High-resolution satellite surface latent heat fluxes in North Atlantic hurricanes. *Mon. Wea. Rev.*, **139**, 2735-2747, doi:10.1175/2011MWR3548.1.

Matricardi, M., and R. Saunders, 1999: Fast radiative transfer model for simulation of infrared atmospheric sounding interferometric radiances. *Appl. Optics*, **38**, 5679-5691, doi:10/1364/AO.38.005679.

McMillin, L.M., J. Zhao, M.K. Rama Varma Raja, S.I. Gutman and J.G. Yoe, 2007: Radiosonde humidity corrections and potential Atmospheric Infrared Souder moisture accuracy. *J. Geophys. Res.*, **112**, D13S90, (1-13), doi:10.1029/2005JD006109.

Miloshevich, L.M., H. Vomel, D.N. Whiteman, B.M. Lesht, F.J. Schmidlin and F. Russo, 2006: Absolute accuracy of water vapor measurements from six operational radiosonde types launched during AWEX-G and implications for AIRS validation. *J. Geophys. Res.*, **111**, D09S10, (1-25), doi:10.1029/2005JD006083.

Murphy, D.M., and T. Koop, 2005: Review of vapour pressures for ice and supercooled water for atmospheric applications. *Quart. J. Roy. Meteor. Soc.*, **131**, 1539-1565, doi:10.1256/qj.04.94.

Noh, Y-C., B-J. Sohn, Y. Kim, S. Joo and W. Bell, 2016: Evaluation of temperature and humidity profiles of Unified Model and ECMWF analyses using GRUAN radiosonde observations. *Atmos.*, **7**, 94, (1-13), doi:10.3390/atmos7070094.

Rossow, W.B., and L.C. Garder, 1993a: Cloud detection using satellite measurements of infrared and visible radiances for ISCCP. *J. Climate*, **6**, 2341-2369.

Rossow, W.B., and L.C. Garder, 1993b: Validation of ISCCP cloud detections. *J. Climate*, **6**, 2370-2393.

Rossow, W.B., and R.A. Schiffer, 1999: Advances in understanding clouds from ISCCP. *Bull. Amer. Meteor. Soc*., **80**, 2261-2287.

Saunders, R., M. Matricardi and P. Brunel, 1999: An improved fast radiative transfer model for assimilation of satellite radiance observations. *Quart. J. Roy. Meteor. Soc.*, **125**, 1407-1425.

Saunders, R., P. Rayer, P. Brunel, A. von Engeln, N. Bormann, L. Strow, S. Hannon, S. Heilliette, Xu Lu, F. Miskolczi, Y. Han, G. Mosiello, J-L. Moncet, Gennady Uymin, V. Sherlock and D.S. Turner, 2007: A comparison of radiative transfer models for simulating Atmospheric Infrared Sounder (AIRS) radiances. *J. Geophys. Res.*, **112**, D01S90, doi:10.1029/2006JD007088.

Seidel, D.J., M. Free and J. Wang, 2005: Diurnal cycle of upper-air temperature estimated from radiosondes. *J. Geophys. Res.*, **110**, D09102, (1-13), doi:10.1029/2004JD005526.

Sherwood, S.C., J.R. Lanzante and C.L. Meyer, 2005: Radiosonde daytime biases and late-20th Century warming. *Science*, **309**, 1556-1559.

Shi, L., 2001: Retrieval of atmospheric temperature profiles from AMSU-A measurement using a neural network approach. *J. Atmos. Ocean Tech.*, **18**, 340-347.

Shi, L., J.J. Bates, X. Li, S.M. Uppala and G. Kelly, 2008: Extending the satellite sounding archive back in time: The vertical temperature profile radiometer data. *J. Appl. Remote Sens.*, **2(1)**, 023506, doi:10.1117/1.2889435.

Shi, L., and J.J. Bates, 2011: Three decades of intersatellite-calibrated High-Resolution Infrared Radiation Sounder upper tropospheric water vapor. *J. Geophys. Res.*, **116**, D04108, doi:10.1029/2010JD014847.

Shi, L., J.L. Matthews, S-P. Ho, Q. Yang and J.J. Bates, 2016: Algorithm development of temperature and humidity profile retrievals for long-term HIRS observations. *Remote Sens.*, **8**, 280, (1-17), doi:10.3390/rs8040280.

Simmons, A., S. Uppala, D. Dee and S Kobayashim 2007: ERA-Interim: New ECMWF reanalysis products from 1989 onwards. *ECMWF Newsletter*, **110**, 26-35.

Smith, A., N. Lott and R. Vose, 2011: The Integrated Surface Database: Recent developments and partnerships. *Bull. Amer. Meteor. Soc.*, **92**, 704-708, doi:10.1175/2011BAMS3015.1.

Sun, B., A. Reale, D.J. Seidel and D.C. Hunt, 2010: Comparing radiosonde and COSMIC atmospheric profile data to quantify differences among radiosonde types and the effects of imperfect collocation on comparison statistics. *J. Geophys. Res.*, **115**, D23104, (1-16), doi:10.1029/2010JD014457.

Susskind, J., C. Barnet, J. Blaisdell, L. Iredell, F. Keita, L. Kouvaris, G. Molnar and M. Chahine, 2006: Accuracy of geophysical parameters derived from Atmospheric Infrared Sounder/Advanced Microwave Sounding Unit as a function of fractional cloud cover. *J. Geophys. Res.*, **111**, D09S17, (1-19), doi:10.1029/2005JD006272.

Vinukollu, R.K., E.F. Wood, C.R. Ferguson and J.B. Fisher, 2011: Global estimates of evapotranspiration for climate studies using multisensory remote sensing data: Evaluation of three process-based approaches. *Remote Sens. Environ.*, **115**, 801-823, doi:10.1016/j.rse.2010.11.006.

Wang, J., D.J. Carlson, D.B. Parsons, T.F. Hock, D. Lauritsen, H.L. Cole, K. Beierle and E. Chamberlain, 2003: Performance of operational radiosonde humidity sensors in direct comparison with a chilled mirror dew-point hygrometer and its climate implication. *Geophys. Res. Lett.*, **30**, 16, 1860, (1-4), doi:10.1029/2003GL016985.

Wang, J., and L. Zhang, 2008: Systematic errors in global radiosonde precipitable water data from comparisons with ground-based GPS measurements. *J. Climate*, **21**, 2218-2238, doi:10.1175/2007JCLI1944.1.

Zhang, Y-C., W.B. Rossow and A.A. Lacis, 1995: Calculation of surface and top-of-atmosphere radiative fluxes from physical quantities based on ISCCP datasets, Part I: Method and sensitivity to input data uncertainties. *J. Geophys. Res.*, **100**, 1149-1165.

Zhang, Y-C., W.B. Rossow, A.A. Lacis, M.I. Mishchenko and V. Oinas, 2004: Calculation of radiative fluxes from the surface to top-of-atmosphere based on ISCCP and other global datasets: Refinements of the radiative transfer model and the input data. *J. Geophys. Res.*, **109**, doi 10.1029/2003JD004457 (1-27 + 1-25).

Zhang, Y-C., W.B. Rossow and P.W. Stackhouse, 2006: Comparison of different global information sources used in surface radiative flux calculation: Radiative properties of the near-surface atmosphere. *J. Geophys. Res.*, **111**, D01102, doi: 10.1029/2005JD007008, (1-13).

Table 1: List of polar orbiting satellites providing HIRS data and their operational period. Also indicated is the availability of PATMOS-x results to check for cloud contamination.

Satellite	NEW HIRS time record	PATMOS-x time record
M02	12/2/2006-12/31/2014	6/29/2007-12/9/2014
N06	7/13/1979-4/2/1983	6/30/1980-8/19/1981
N07	7/9/1981-1/29/1985	8/24/1981-2/1/1985
N08	4/30/1983-6/1/1984	5/16/1983-10/13/1985
N09	1/1/1985-10/19/1988	2/25/1985-11/6/1988
N10	11/28/1986-8/27/1991	11/17/1987-9/16/1990
N11	10/14/1988-12/30/1994	11/8/1988-8/31/1994
N12	6/1/1991-3/31/1997	9/16/1991-12/14/1998
N14	1/30/1995-7/28/2005	2/9/1995-7/25/2002
N15	10/27/1998-3/30/2005	10/26/1998-12/9/2014
N16	3/1/2001-12/31/2003	3/20/2001-7/19/2006
N17	7/16/2002-3/20/2013	8/24/2002-1/10-2009
N18	X	7/19/2005-12/9/2014
N19	X	4/19/2009-12/9/2014
TIROS-N	X	1/1/1979-1/19/1980

Table 2: Pressure (mb) levels used in the New HIRS, SWOOSH and NNHIRS data products.

New Hirs	1000, 850, 700, 600, 500, 400, 300, 200, 100, 50
Swoosh	316.2278, 261.0157, 215.4435, 177.8279, 146.7799, 121.1528, 100.0, 82.540, 68.1292, 46.41589, 38.31187, 31.62278, 26.10157, 21.54435, 17.7827, 14.67799, 12.11528, 10.0, 8.254042, 6.812921, 5.623413, 4.641589, 3.831187, 3.162278, 2.610157, 1.778279, 1.467799, 1.211528,1.0
NNHIRS	Surface, 900, 800, 740, 680, 620, 560, 500, 440, 380, 320, 200, 150, 100, 50, 10

Table 3: Surface Type code values and definitions from the ISCCP SURFACETYPE product together with "window" IR surface emissitivies assigned to each type.

Surface Type Code	Description	IRemiss
0	Water	0.990
1	Evergreen Needleleaf Forest	0.985
2	Evergreen Broadleaf Forest	0.980
3	Deciduous Needleleaf Forest	0.985
4	Deciduous Broadleaf Forest	0.980
5	Mixed Forest	0.985
6	Closed Shrubland	0.980
7	Open Shrubland	0.975
8	Woody Savanna	0.980
9	Savanna	0.980
10	Grassland	0.980
11	Permanent Wetland	0.980
12	Cropland	0.980
13	Urban and Built-up	0.980
14	Cropland/Natural Vegetation Mosaic	0.980
15	Permanent Snow and Ice (Glaciers)	0.990
16	Barren or Sparsely Vegetated	0.965
17	Unclassified	0.980
18	Permanent Ice Shelf	0.990

Table 4: ISD-based additive adjustments applied to land TA values from New HIRS to produce the NNHIRS product, based on empirical fits to the global monthly data illustrated in Figure 2.

Month	Temp<	Formula (Ta+)	Temp between	Formula	Temp >	Formula
January	244	0.3857002519*ta – 94.5032049617	>244&<295	-0.0054097694 *(ta^2) +2.9125939259*ta - 388.4916046312	295	-0.1518243949 *ta +44.0305015119
February	239	0.2904500663*ta-69.8797243893	>239 &<293	-0.0054506843 *ta^2 +2.9003645951*ta - 381.7292974161	293	-0.2036320737 *ta +58.8812629801
March	228	0.1929249606*ta - 44.0568465378	>228 &<294	-0.0045889045 *ta^2 +2.3972297270*ta - 308.1724536587	295	-0.2166178463 *ta +63.1033958409
April	210	0.1324798470*ta - 27.7097642834	>210 &<299	-0.0028239784 *ta^2 +1.4352990071*ta - 176.7596947726	299	-0.1807989857 *ta +53.7622617563
May	217	0.0981604904*ta-18.9647099343	>217 &<296	-0.0040166274 *ta^2 +2.0625570246*ta - 258.4956821271	296	-0.2415170461 *ta +71.1131718104
June	210	0.1640082372*ta-33.8080845539	>210 &<298	-0.0034019831 *ta^2 +1.7291929471*ta-	298	-0.2153255282 *ta+63.8890704900

				213.1600759454		
July	207	0.1419663098*ta - 28.1787714486	>207 &<298	-0.0031408833*ta^2 +1.5864432206*ta - 193.6949386353	298	-0.2038138199*ta +60.6835506916
August	204	0.1961498547*ta- 40.2241299299	>204 &<299	-0.0033120951*ta^2 +1.6648981584*ta - 201.818862609	299	-0.1871380553*ta +55.8782944215
September	212	0.1708540573*ta - 34.9000070844	>212 &<295	-0.0045005593*ta^2 +2.2801804787*ta - 28.0070266930	295	-0.2916077704*ta +85.2141076261
October	209	0.1407779662*ta – 28.2261622686	>209 &<294	-0.0038523629*ta^2 +1.9387707020*ta - 237.0246064576	294	-0.2376603006*ta +69.2794313298
November	228	0.2364392082*ta - 55.434758346	>228 &<293	-0.0040196954*ta^2 +2.0959372357*ta - 268.9476735128	293	-0.1976990939*ta +57.2210979996
December	241	0.3266645793*ta – 79.49309416	>241 &<293	-0.0053380406*ta^2 +2.8535980471*ta - 377.746669059	293	-0.1747278096*ta +50.4574170153

Table 5: Sample summary comparison of NNHIRS values matched (see text for match-up specifications) to values from ARSA (over land), AIRS and ERA-I for January (indicated by 01) and July (indicated by 07) 2007: values are temperature and specific humidity at the surface, 900 mb, 500 mb and 320 mb levels (TA, T900, T500, T320, QA, Q900, Q500, Q320, respectively). The first number in each column is the mean difference (Other minus NNHIRS) over the domain and whole month and the second number is the rms difference.

		Ocean			Land		
	Avg	AIRS	ERA-I	Avg	AIRS	ERA-I	ARSA
TA-01	288	-0.6/1.8	+0.2/1.7	277	+0.2/2.9	0/3.4	+0.7 /3.3
TA-07	288	-0.1/1.7	+0.4/1.9	277	-2.1/3.3	-1.8/3.1	-0.6 /2.6
T900-01	285	-1.6/2.2	-1.5/2.5	279	+1.4/2.7	+1.7/3.5	+2.1 /3.4
T900-07	291	-1.4/2.5	-1.3/2.5	285	+0.4/2.5	+0.3/2.9	+0.9 /2.9
T500-01	258	+0.8/1.8	+0.6/1.7	252	+1.4/1.4	+1.4/1.3	+0.26/1.5
T500-07	256	+0.7/1.2	+0.5/1.4	256	+0.9/1.4	+0.7/1.4	-0.4/1.2
T320-01	236	+1.1/1.7	+1.3/1.8	232	+1.3/+1.3	+1.3/1.4	+0.8/1.7
T320-07	236	+0.7/1.2	+1.1/1.2	238	+0.9/1.2	+1.3/1.2	+1.9/1.2
QA-01	11.4	-1.0/0.9	-1.5/1.2	5.3	+0.6/1.8	+0.4/1.8	
QA-07	11.3	-0.3/1.0	-1.2/1.2	6.7	+0.9/1.9	+0.4/1.7	
Q900-01	6.8	-1.0/0.9	+1.2/1.3	2.9	+1.2/1.8	+1.5/1.9	+1.1/1.2
Q900-07	7.3	-0.3/1.0	+0.8/1.1	5.3	+1.6/1.6	+1.6/1.5	+1.4/+1.5
Q500-01	0.72	+0.2/0.4	+0.4/0.5	0.71	+0.2/0.6	+0.3/0.6	+0.2/+0.5
Q500-07	0.76	+0.2/0.4	+0.3/0.4	0.89	+0.3/0.5	+0.5/0.6	+0.4/0.5
Q320-01	0.17	+0.06/0.2	+0.2/0.2	0.14	+0.06/0.23	+0.1/0.2	+0.09/0.2
Q320-07	0.18	0.0/0.01	+0.1/0.2	0.20	+0.07/0.21	+0.2/0.2	+0.19/0.25

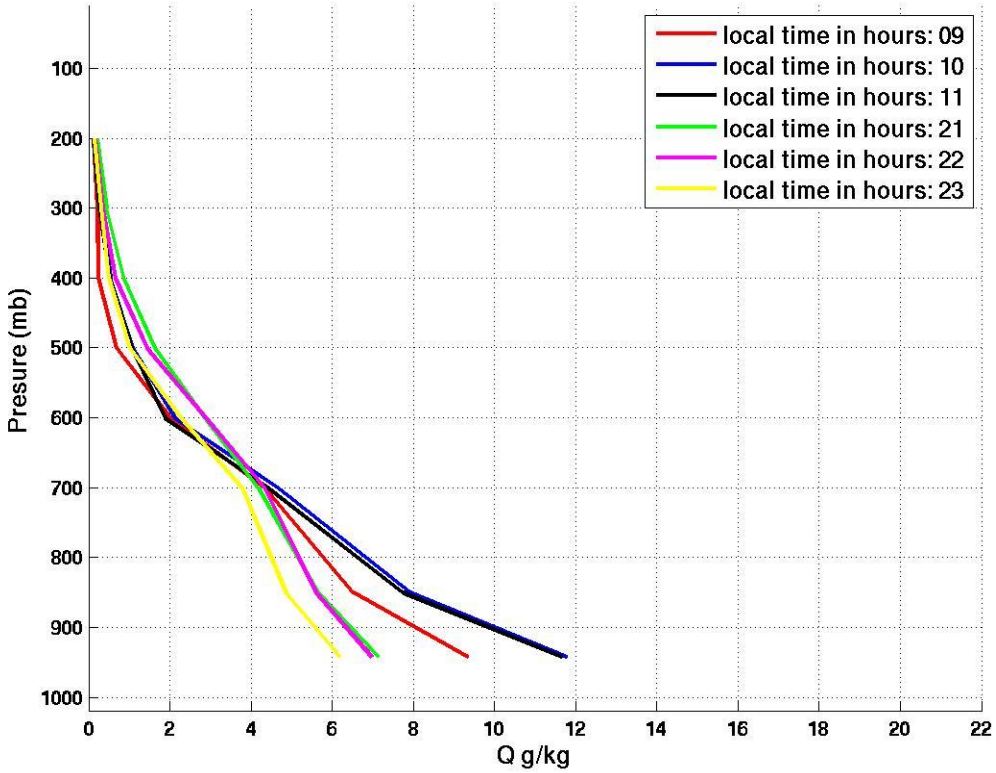

FIGURE 1: Sample New HIRS profile of Q over the Sahara desert at different local times of day

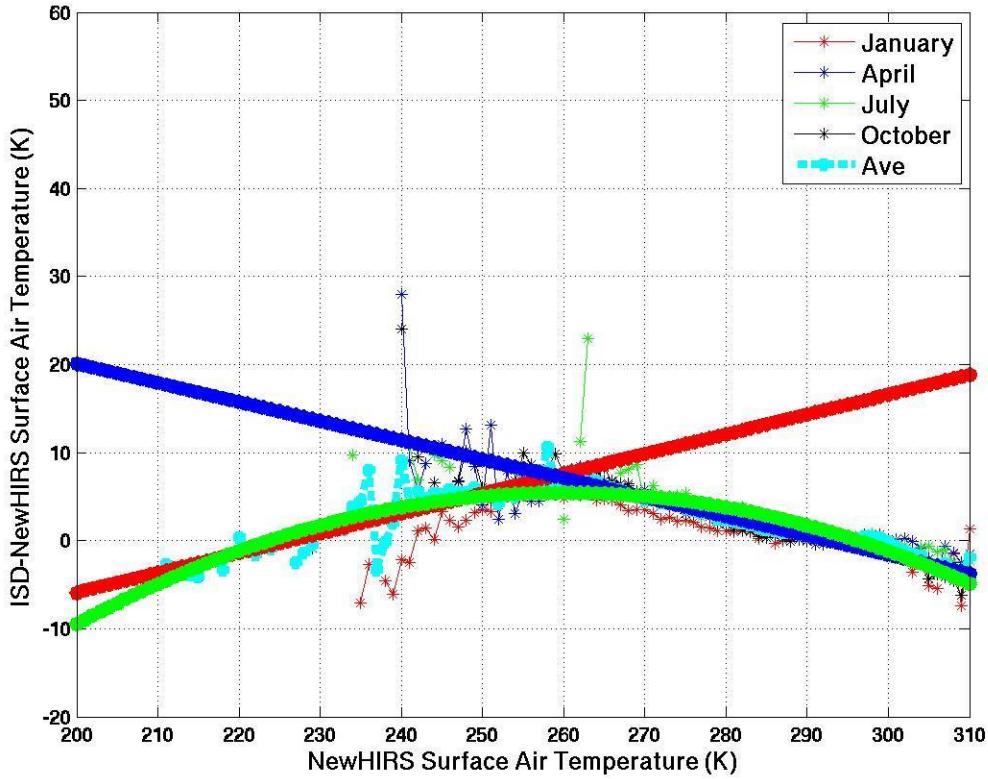

FIGURE 2. Annual average difference of TA values (in Kelvins) from New HIRS matched (see text for match up specifications) with ISD values as a function of New HIRS TA.

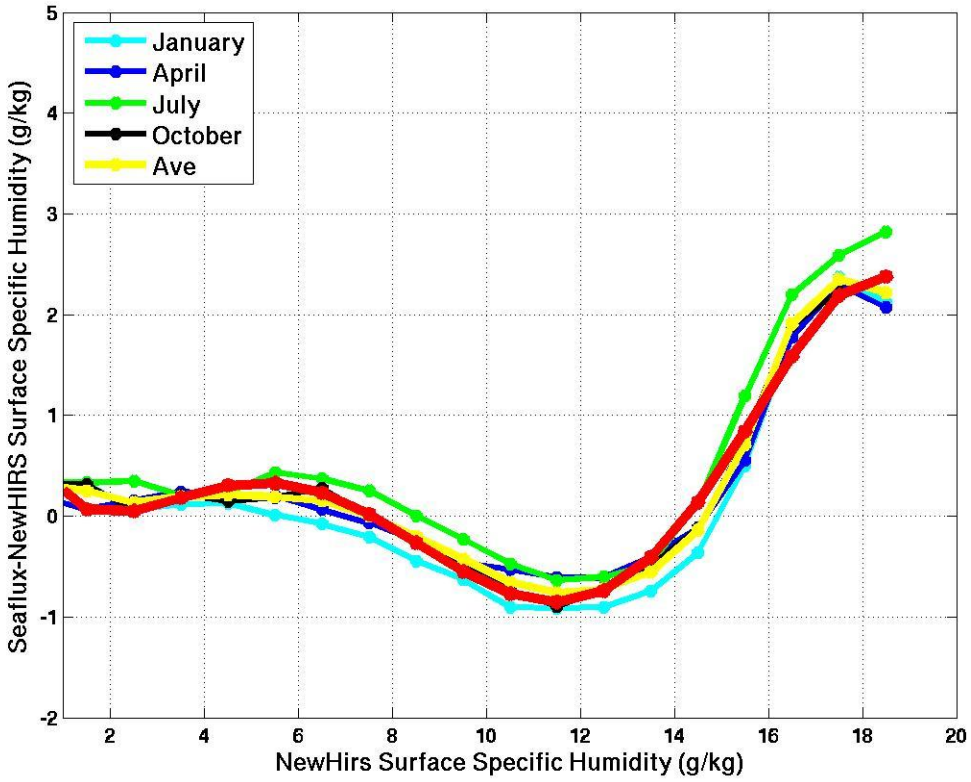

Figure 3: Annual average difference of QA values (in g/kg) from New HIRS matched (see text for match-up specifications) to SeaFlux values as a function of New HIRS QA.

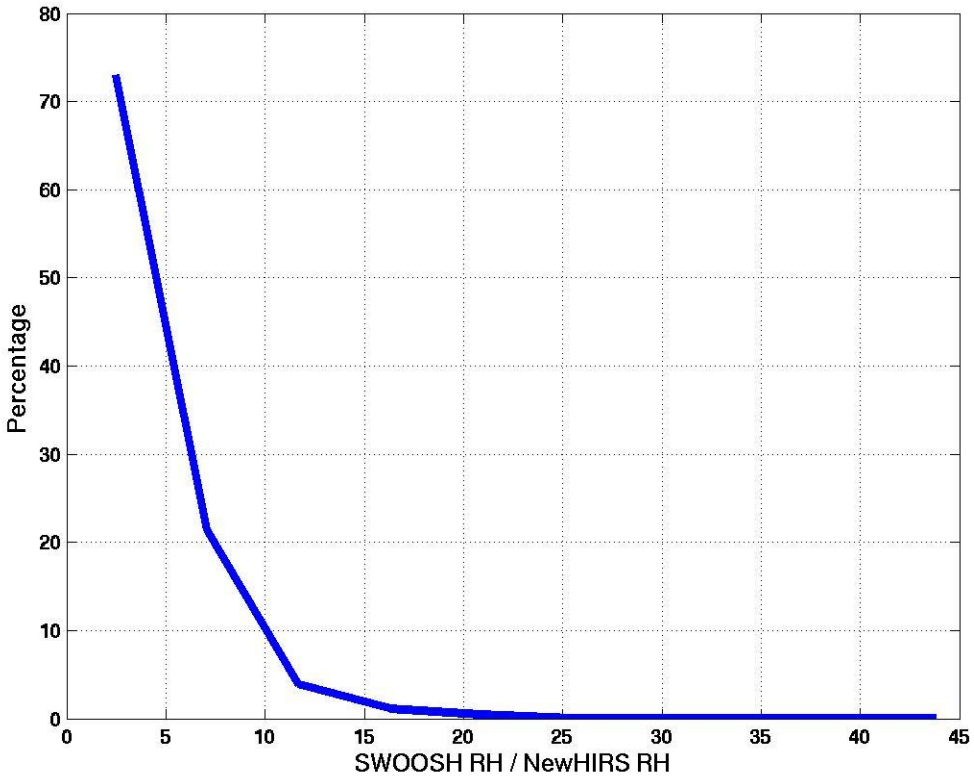

Figure 4: Frequency distribution of the ratio of matched (see text for match-up specifications) relative humidity values from SWOOSH and New HIRS at the 320 mb level.

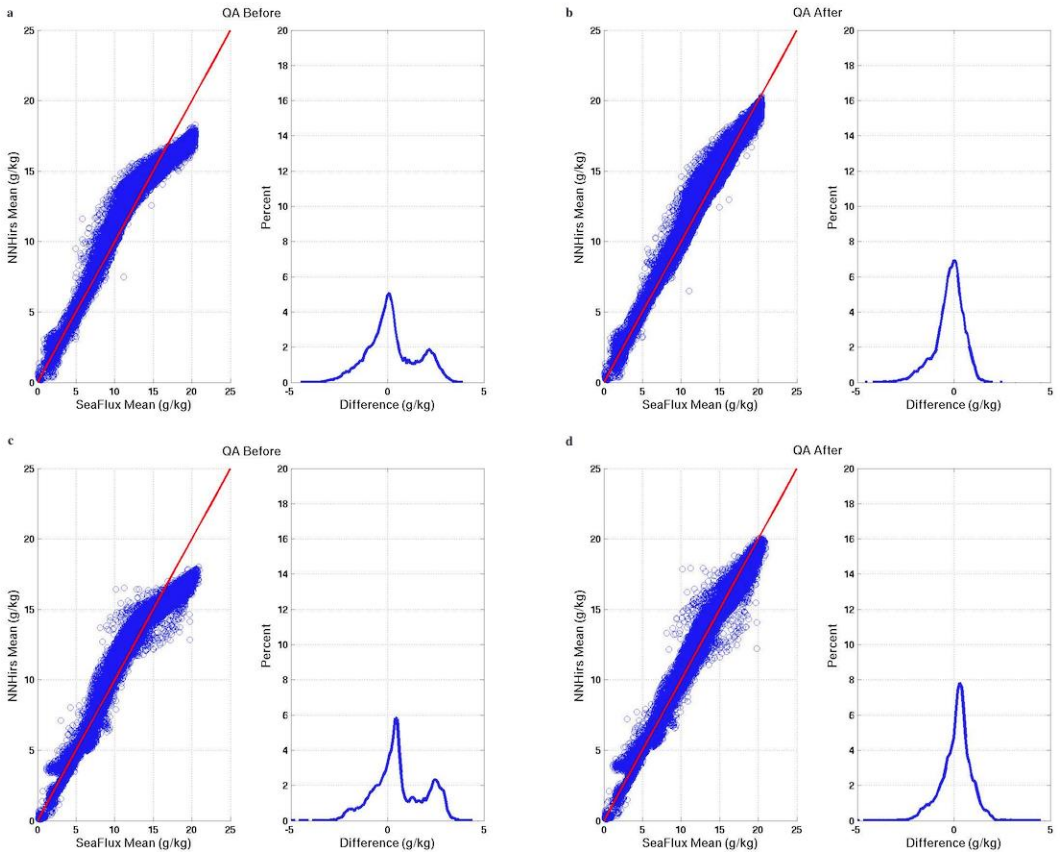

Figure 5: Scatterplots of spatially matched monthly mean QA values (g/kg) and histograms of differences (g/kg) from New HIRS before (a, b, respectively) and after (c, d, respectively) the application of the SeaFlux-based adjustment as compared to SeaFlux values.

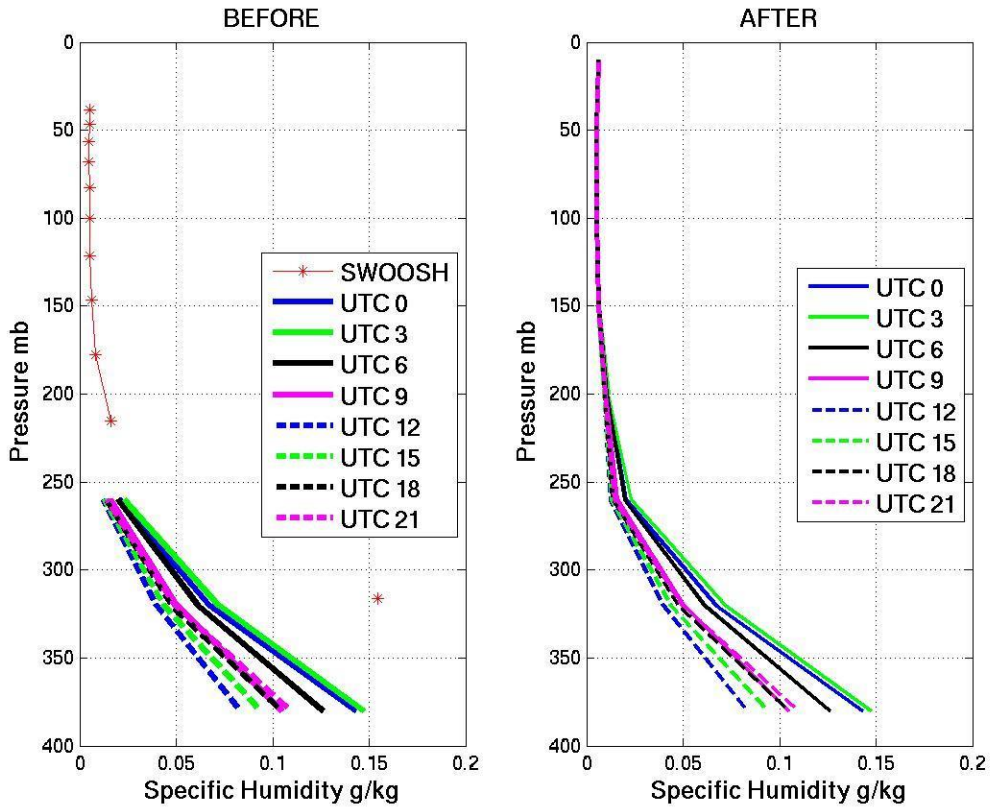

Figure 6: Example of the reconciliation of the vertical profiles of Q (in g/kg) from New HIRS and SWOOSH at different times of day.

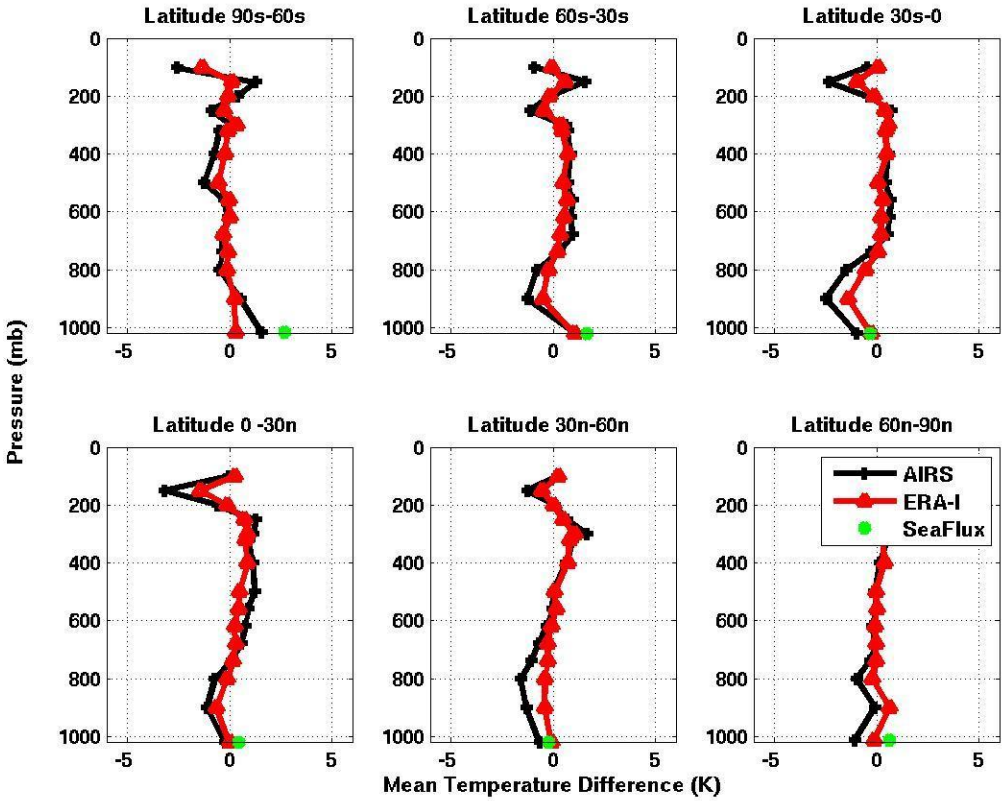

Figure 7: Monthly average difference (Other minus NNHIRS) of T profiles (in Kelvins) over ocean compared to matched (see text for match-up specifications) values from AIRS (black) and ERA-I (red) for July 2007 in six latitude zones. The green dot indicates the average difference at the surface with SeaFlux.

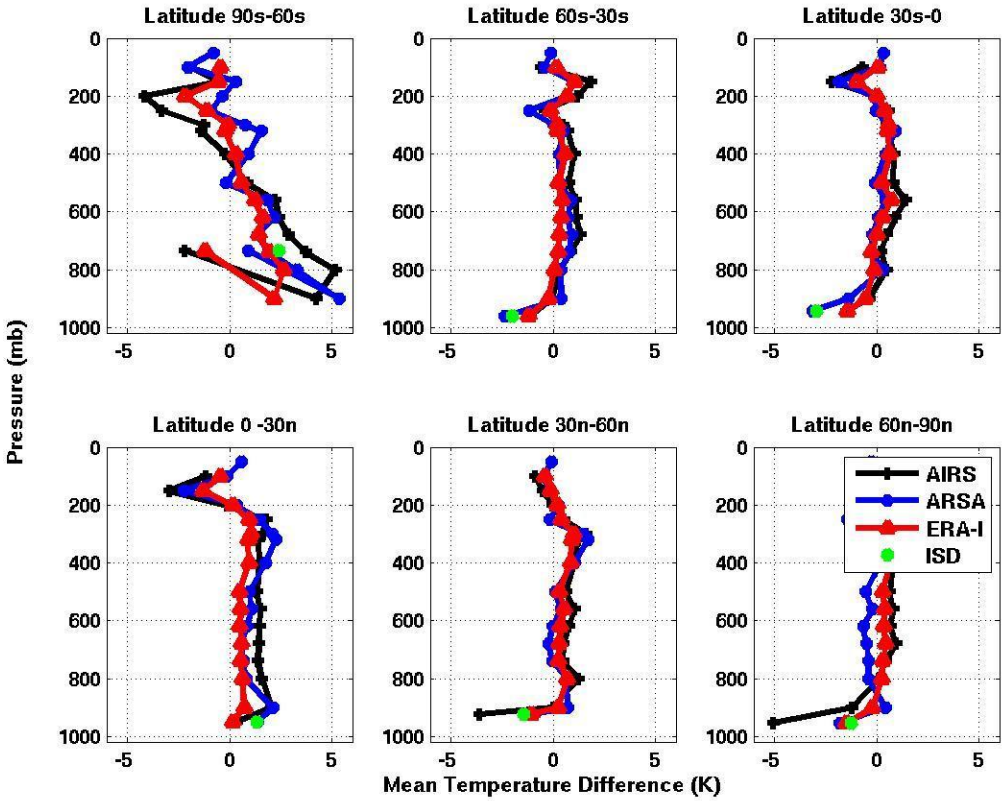

Figure 8: Monthly average difference (Other minus NNHIRS) of T profiles (in Kelvins) over land compared to matched (see text for match-up specifications) values from AIRS (black), ARSA (blue) and ERA-I (red) for July 2007 in six latitude zones. The green dot indicates the average difference at the surface with ISD.

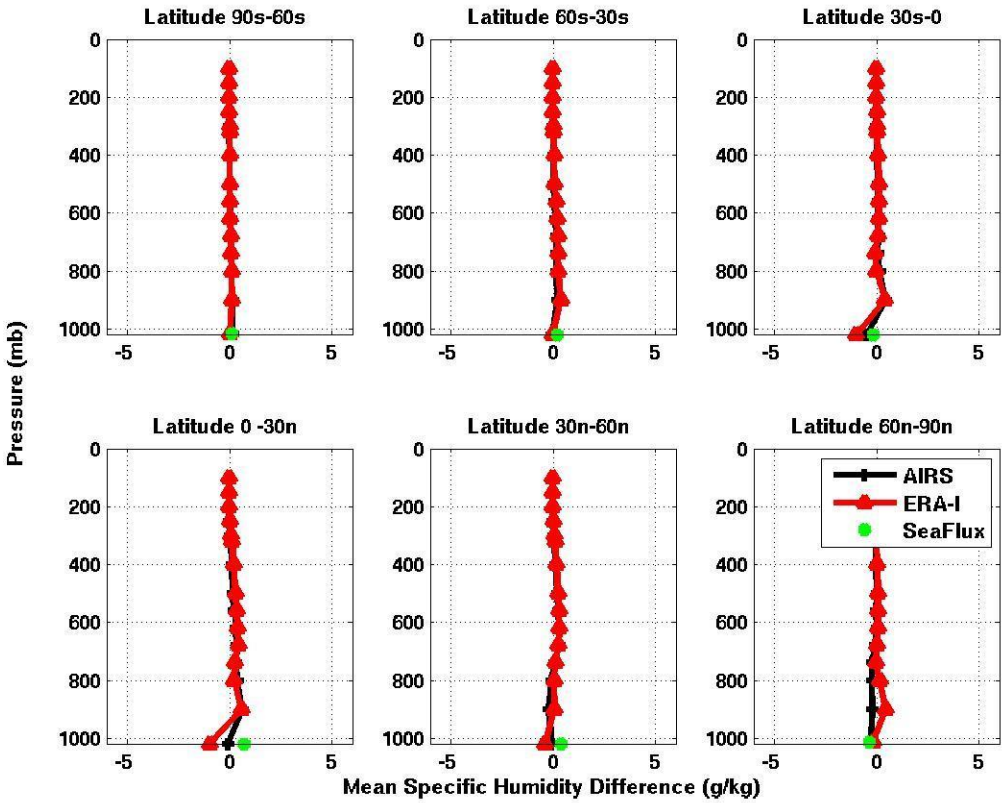

Figure 9: Monthly average difference (Other minus NNHIRS) of Q (in g/kg) profiles over ocean compared to matched (see text for match-up specifications) values from AIRS (black) and ERA-I (red) for July 2007 in six latitude zones. The green dot indicates the average difference at the surface with SeaFlux.

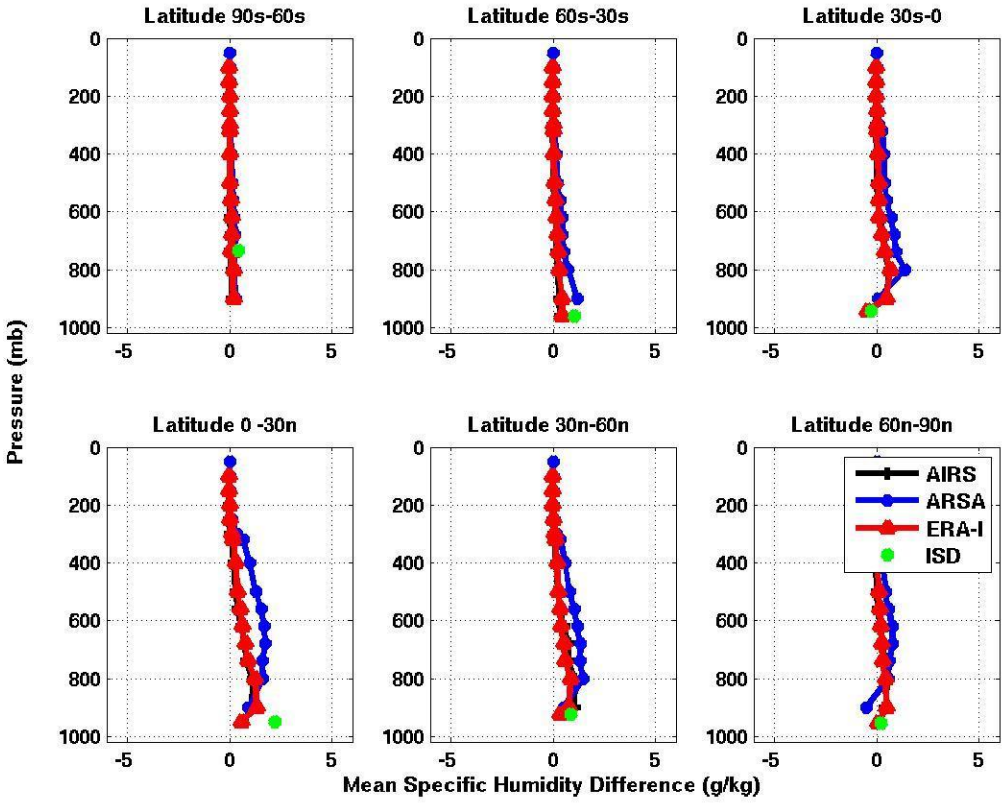

Figure 10: Monthly average difference (Other minus NNHIRS) of Q profiles (in g/kg) over land compared to matched (see text for match-up specifications) values from AIRS (black), ARSA (blue) and ERA-I (red) for July 2007 in six latitude zones. The green dot indicates the average difference at the surface with ISD.

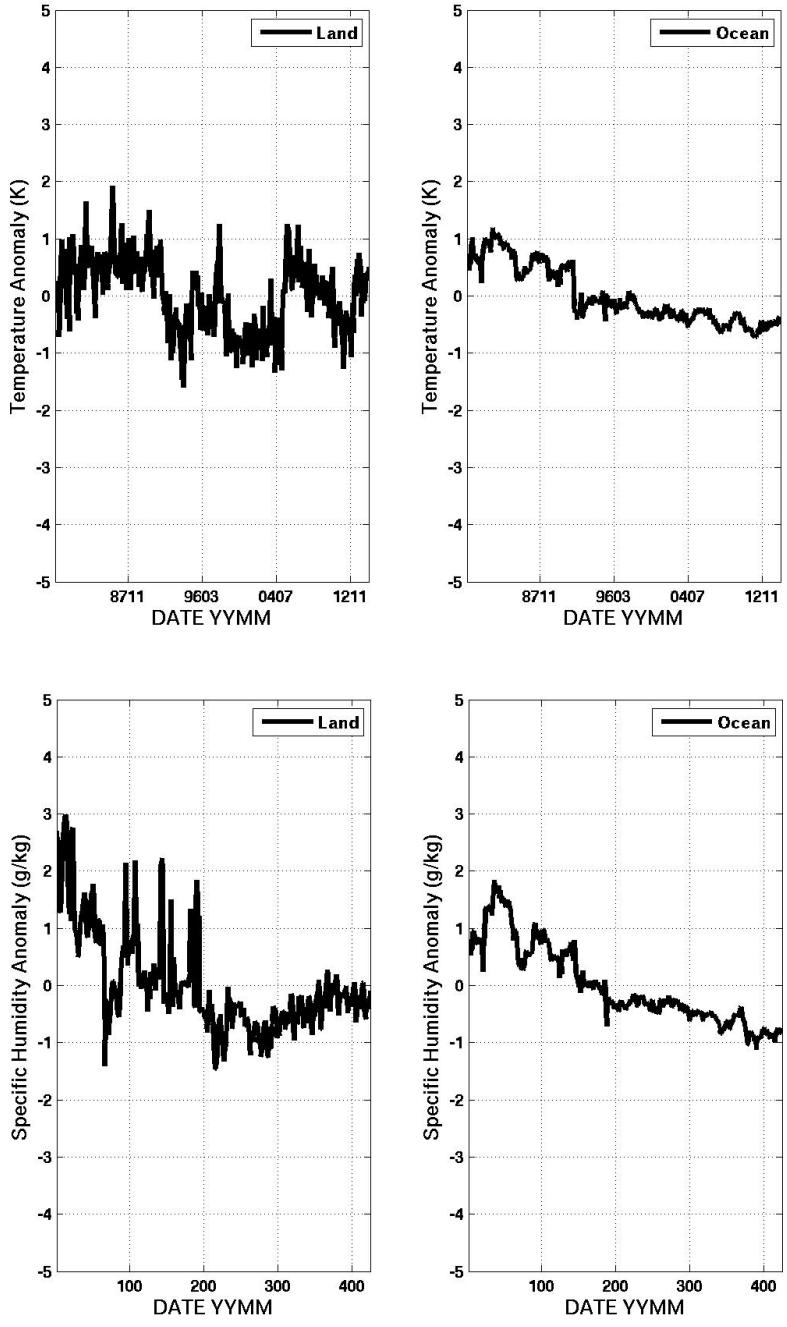

Figure 11: Deseasonalized anomalies of global monthly mean TA over land and ocean for the whole NNHIRS time record (1980-2014).